International Immunopharmacology 118 (2023) 110065

Contents lists available at ScienceDirect

International Immunopharmacology

journal homepage: www.elsevier.com/locate/intimp

Tanshinone IIA analogue 15a inhibits NLRP3-mediated inflammation by activating mitophagy in macrophages to alleviate acute tubular necrosis

Jiahao Chen [a,b], Wu Luo [a,b], Chenghong Hu [b], Miao Ren [b], Haowen Xu [b], Xiangwei Xu [a], Weifeng Li [b], Yue Chen [b], Jingjing Shao [a,b], Zhongxiang Xiao [c], Xinting Lv [a,*], Guang Liang [a,b,*]

[a] Affiliated Yongkang First People's Hospital and School of Pharmacy, Hangzhou Medical College, Hangzhou, Zhejiang 310012, China
[b] Chemical Biology Research Center, School of Pharmaceutical Sciences, Wenzhou Medical University, Wenzhou, Zhejiang, 325035, China
[c] Affiliated Yueqing Hospital,Wenzhou Medical University, Yueqing, Wenzhou, Zhejiang, 325035, China

ARTICLE INFO

Keywords:
Tanshinone IIA
Mitophagy
mtROS
NLRP3
Macrophage
Acute tubular necrosis

ABSTRACT

Background: Acute tubular necrosis (ATN) is a common type of acute renal failure. Recent studies have shown that NOD-like receptor family pyrin domain-containing 3 (NLRP3) inflammasome-mediated pyroptosis in macrophages plays a crucial role in the progression of ATN. Previously, we synthesized an anti-inflammatory compound 15a based on Tanshinone IIA (Tan IIA). In the present study, we found that compound 15a exhibited a greater inhibitory effect on NLRP3-mediated pyroptosis than Tan IIA in vitro.

Methods: C57BL/6 and NLRP3-knockout (NLRP3-KO) mice were intraperitoneally injected with LPS or folic acid (FA) to develop ATN. In vitro, bone marrow-derived macrophages (BMDMs) were treated with LPS for 3 h and then treated with ATP for 0.5 h.

Results: We explored the mechanism by which compound 15a inhibited NLRP3 inflammasome in BMDMs as well as its renal protective effect against ATN in mice. We found that compound 15a exhibited a protective effect on mitochondria and reduced the production of mitochondrial reactive oxygen species (mtROS). Moreover, we revealed that compound 15a remarkably reduced the production of mtROS by promoting mitophagy, which resulted in the inhibition of NLRP3 inflammasome to alleviates ATN in mice.

Conclusion: In summary, compound 15a inhibited NLRP3-mediated inflammation by activating mitophagy in macrophages to alleviate ATN. Our results identified compound 15a as a promising candidate for the treatment of NLRP3-driven ATN.

1. Introduction

Acute tubular necrosis (ATN) is very common in the clinic, which is caused with multiple factors including septicopyemia, nephrotoxic lesions, and ischemia–reperfusion injury. Although the treatment of the disease has been greatly improved with continuous research on the pathogenesis of ATN in the past three decades, the rate of clinical mortality remains as high as 50–80 % [1]. In recent years, inflammation has been shown to have a significant impact on ATN [2–4]. Infiltrated macrophages play various roles in different stages of ATN [5]. Macrophages aggravate the inflammatory cascade response and recruit leukocytes at the early stage of ATN, and the cells also exhibit restorative effect at the later stage [5–8]. Inflammatory activation in macrophages is the key producers of IL-1β in the initial response to necrotic cells [4]. Recent studies have identified an important role of NOD-like receptor family pyrin domain-containing 3 (NLRP3)-mediated pyroptosis in ATN [5,9–12]. NLRP3 is a pattern recognition receptor (PRRs) in the cytoplasm. Once assembled and activated in the presence of immune

Abbreviations: ATN, Acute tubular necrosis; BUN, Blood urea nitrogen; BMDMs, Bone marrow-derived macrophages; COX IV, Cytochrome *c* oxidase IV COX IV; FA, Folic acid; H&E, Hematoxylin and Eosin; IL-1β, Interleukin 1β; IL-18, Interleukin 18; LDH, Lactate dehydrogenase; LRR, Leucine-rich repeat domain; LPS, Lipopolysaccharide; mtROS, Mitochondrial reactive oxygen species; NLRP3-KO, NLRP3 knockout; NLRP3, NOD-like receptor family pyrin domain-containing 3; OCT, Optimal Cutting Temperature; PRRs, Pattern recognition receptors; PAS, Periodic-acid-schiff; Pink1, PTEN-induced kinase 1; SCr, Serum creatinine; Tan IIA, Tanshinone IIA; WT, Wild type.

* Corresponding authors at: Affiliated Yongkang First People's Hospital and School of Pharmacy, Hangzhou Medical College, Hangzhou, Zhejiang 310012, China (Guang Liang) Affiliated Yongkang First People's Hospital, Hangzhou Medical College, Hangzhou, Zhejiang 310012, China(Xinting Lv).
E-mail addresses: yklvxinting@163.com (X. Lv), wzmclangguang@163.com (G. Liang).

https://doi.org/10.1016/j.intimp.2023.110065
Received 28 January 2023; Received in revised form 13 March 2023; Accepted 20 March 2023

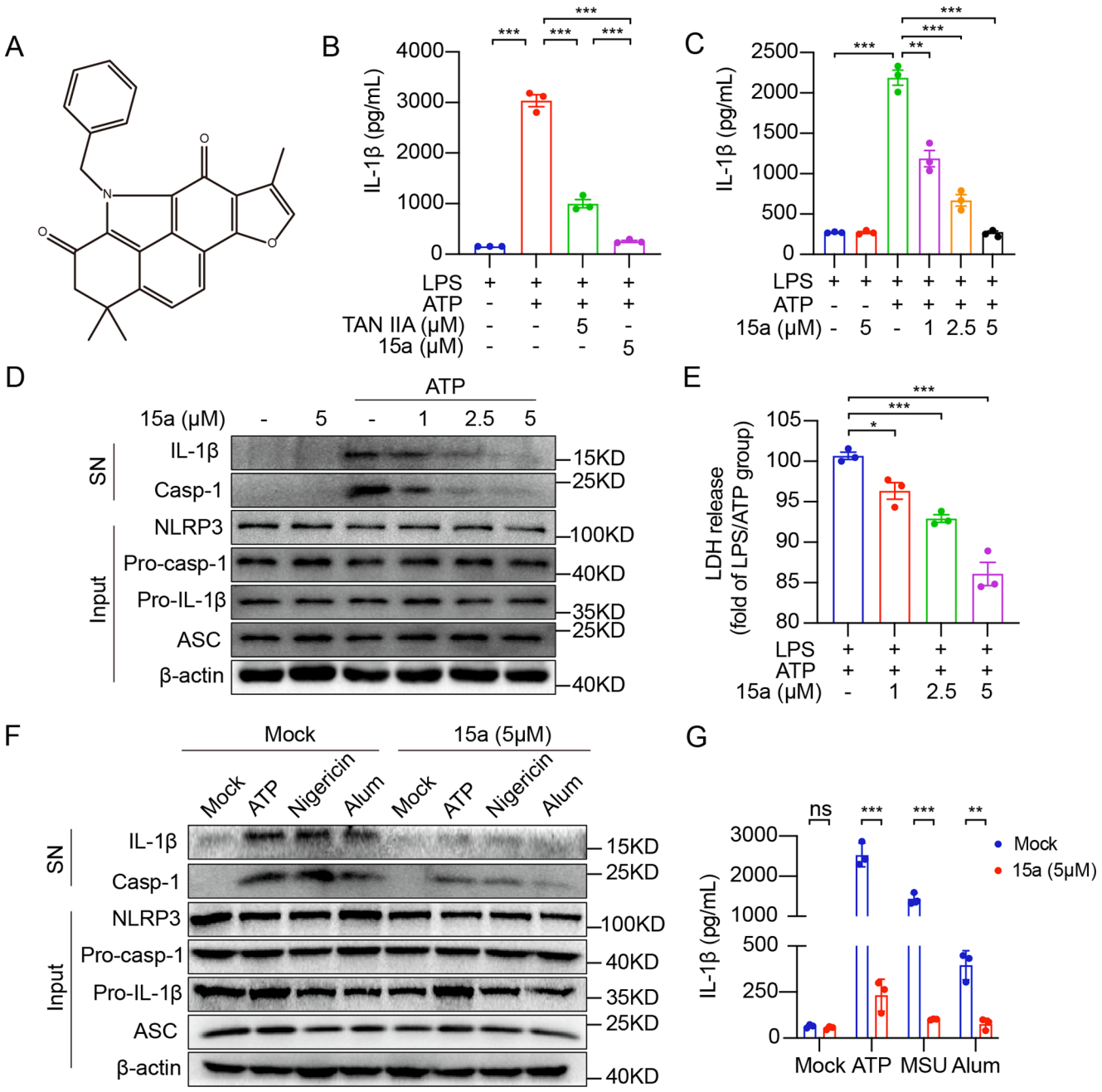

Fig. 1. Compound 15a significantly inhibits NLRP3-mediated pyroptosis in BMDMs. (A) The chemical structure of compound 15a. **(B)** ELISA of IL-1β in supernatant of LPS/ATP-challenged BMDMs treated with tanshinone IIA (5 μM) or compound 15a (5 μM) for 0.5 h. **(C)** Detection of IL-1β released in the supernatant using ELISA assay. **(D)** Western blotting analysis of the levels of IL-1β and casp-1 released in the culture supernatant and that of NLRP3, pro-IL-1β, pro-caspase-1, ASC, and β-actin in the lysates of BMDMs. **(E)** Assay of LDH release in the supernatants of LPS-primed BMDMs treated with compound 15a (1, 2.5, 5 μM) for 0.5 h and stimulated with ATP for 0.5 h. **(F, G)** LPS-primed BMDMs were treated with or without compound 15a (5 μM) for 0.5 h and then challenged with ATP for 0.5 h, nigericin for 0.5 h, or alum for 4 h. Western blot of cleaved IL-1β and casp-1 in the supernatant **(F)** and ELISA of cleaved IL-1β in the supernatant **(G)**. Data are presented as the mean ± SEM, n = 3; *P < 0.05, **P < 0.01, ***P < 0.001; ns, not significant.

activators such as pathogen-associated molecular patterns (PAMPs) and danger-associated molecular patterns (DAMPs), the NLRP3-ASC-caspase-1 protein complex, which is named the NLRP3 inflammasome, induces self-cleavage of caspase-1, leading to the maturation and release of the pro-inflammatory cytokines interleukin 1β (IL-1β) and interleukin 18 (IL-18) in macrophages [13–15]. Thus, small molecules suppressing NLRP3 may provide new therapeutic strategies for ATN.

Studies have revealed that mitochondrial reactive oxygen species (mtROS) is one of the upstream regulators of NLRP3 inflammasome. Along with performing critical functions, mitochondria activation may potentially harm cells by producing excessive mtROS. When mtROS are constantly challenged with intracellular and extracellular stimulation, they eventually induce structural and functional failure in cells [16]. Although the exact mechanism is not fully elucidated, mitochondrial dysfunction and mtROS release are important triggers for NLRP3 inflammasome activation and pyroptosis induction [15,17]. To maintain mitochondrial fitness, the autophagic system targets impaired mitochondria and delivers them to the lysosomes for degradation. This process, called mitophagy, is a fundamental mechanism that regulates mitochondrial quality and quantity and down-regulates the level of

mtROS [17,18]. Hence, mitophagy plays a protective role in pyroptosis by removing NLRP3 activators such as mtROS and damaged mitochondria [19]. However, few studies have reported the role of mitophagy in the pathological regulation of ATN.

Tanshinone IIA (Tan IIA) is a main active ingredient in Salviae miltiorrhiza, a traditional chinese medicinal herb mainly distributed in the Anhui, Shanxi, Shandong, and Jiangsu provinces in China. Tan IIA is traditionally used for treating cardiovascular diseases, diabetes, apoplexy, arthritis, sepsis [20]. Previously, we designed and synthesized a series of Tan IIA-derived compounds, among which, compound 15a (Fig. 1A) showed the most outstanding anti-inflammatory effect in LPS-induced acute lung injury [21]. Therefore, compound 15a was selected for further study and development as a new candidate in inflammatory diseases. However, the molecular mechanism by which compounds 15a exerts anti-inflammatory effects remains unclear. In the current study, we observed that compound 15a exhibited a stronger effect than Tan IIA in suppressing NLRP3-mediated pyroptosis in macrophages. Interestingly, we discovered that compound 15a exerted a protective effect on mitochondria and decreased mtROS formation through the mitophagy-promoting mechanism. By promoting mitophagy to inhibit NLRP3 inflammasome, compound 15a significantly attenuated ATN in two mouse models.

2. Materials and methods

2.1. Chemical and reagents

Compound 15a was synthesized in our laboratory. 15a was dissolved in dimethyl sulfoxide (DMSO) for studies in vitro. In vivo studies, 15a was dissolved in 5 % Tween 80 and PBS. Antibodies against NLRP3 (cat# AG-20B-0014) and caspase-1 (cat# AG-20B-0042) were purchased from Adiopogen (San Diego, CA, USA). Antibody against IL-1β (cat# AF-401-NA) was purchased from R&D Systems (Minneapolis, MN, USA). Antibodies against Flag (cat# 20543–1-AP), HA (cat# 66006–2-Ig), and β-actin (cat# 66009–1-Ig) were purchased from Proteintech (Rosemont, IL, USA). Antibody against NEK7 (cat# ab133514) was purchased from Abcam (Cambridge, UK). Antibodies against Pink1 (cat# 6946 T) and SQSTM1 (cat# 23214S) were obtained from Cell Signaling Technology (Massachusetts, USA).Antibodies against COX IV (cat# T40110S) and LC3B (cat# 83506S) were purchased from Abmart (Hangzhou, China). Lipopolysaccharides (LPS, cat# L2880), adenosine triphosphate (ATP, cat# A3377), and aluminum potassium sulfate dodecahydrate (Alum, cat# 237086) were obtained from Sigma-Aldrich (St.Louis, MO, USA). ATP Assay Kit(cat# S0026B), Tissue Mitochondria Isolation Kit (cat# C3606), and Protein A + G agarose (cat# P2012) were supplied by Beyotime (Shanghai, China). Tanshinone IIA (cat# HY-N0135) was purchased from MedChemExpress (MCE, New Jersey, USA).

2.2. Cell culture

Bone marrow-derived macrophages (BMDMs) were isolated and cultured as described previously [22]. Briefly, the bone marrow cells were flushed out from the femurs and tibias of an 8-week-old C57BL/6J and NLRP3 knockout (NLRP3-KO) mice and were cultured in a medium comprising of 70 % Dulbecco's modified Eagle's medium (DMEM; cat# C11995500BT, Gibco, Waltham, MA, USA), 10 % fetal bovine serum (FBS; cat# 10270–106, Gibco, Waltham, MA, USA), 20 % supernatants of L929 mouse fibroblasts, 10 % FBS and 100 U/mL penicillin, and 100 μg/mL streptomycin (cat# C100C5, NCM Biotech, Suzhou, China) for 7 days. 4 mL of extra fresh culture medium was added to continuously promote cell differentiation on 3th and 5th day. The BMDMs were plated and prepared for subsequent experiments on 7th day.

HEK-293 T cells (cat# GNHu17, Shanghai Institute of Biochemistry and Cell Biology, Shanghai, China) were cultured in DMEM supplemented with 10 % FBS and a penicillin–streptomycin solution. On 3th day, the cells were plated and prepared for subsequent experiments.

L929 mouse fibroblasts (cat# GNM28, Shanghai Institute of Biochemistry and Cell Biology, Shanghai, China) were cultured in minimum essential medium-α (MEM-α; cat# sh30265.01, HyClone, Logan, UT, USA) supplemented with 10 % FBS and a penicillin–streptomycin solution. On 3th day, the culture medium was collected and filtered for culturing BMDMs.

2.3. Mouse models of ATN

All the mouse study protocols were approved by the Wenzhou Medical University Animal Policy and Welfare Committee (approval no.: wydw-2021–147). All experiments were performed at Wenzhou Medical University in accordance with the National Institutes of Health (USA) guidelines. Wildtype C57BL/6 male mice aged 8 weeks were obtained from GemPharmatech (Nanjing, China). NLRP3-KO male mice with a C57BL/6 background (strain No.: VSM40005) were purchased from Beijing Viewsolid Biotech Co., ltd. (Beijing, China). Mice were fed a standard rodent diet and housed under a 12:12 h light–dark cycle at 22 °C.

Mouse models of ATN have been developed using various agents including lipopolysaccharide (LPS), and folic acid (FA) [9]. To investigate the role of compound 15a in ATN, C57BL/6 and NLRP3-KO mice were injected intraperitoneally with compound 15a (5 mg/kg) or PBS with 5 % Tween 80 hourly for twice. Subsequently, the mice were intraperitoneally injected with LPS (10 mg/kg) for 24 h or FA (250 mg/kg) for 36 h to induce ATN [9]. The weight of the mice was measured before the first injection, and the mice were sacrificed. Then, the blood was collected for estimation of serum creatinine (SCr), blood urea nitrogen (BUN), and serum cytokines IL-1β using assay kits (Urea Assay Kit; cat# C013-2–1, Jiancheng Bioengineering Institute, Nanjing, China; Creatinine Assay kit; cat# C011-2–1, Jiancheng Bioengineering Institute, Nanjing, China). Kidney tissues were dissected immediately after isolation. Part of the kidneys was fixed in Optimal Cutting Temperature (OCT) media and 4 % paraformaldehyde. Tissues samples (10 mg) from the remaining part were weighted and prepared for western blotting.

2.4. Tissue staining methods and histological scores

Kidney tissues were fixed in 4 % paraformaldehyde, embedded in paraffin, and sections were stained using H&E kit (cat# G1120, Solarbio, Beijing, China) and PAS kit (cat# G1285, Solarbio, Beijing, China) according to the manufacturer's protocols. The histological score for H&E staining was determined by the Paller scoring method [23]. Ten injured tubules were randomly selected for each high-power field and scored as 100 tubules (100 points). Additionally, we assigned scores for the following characteristics: obvious dilatation of renal tubules, and cell flattening (1 point), brush border injury (1 point), brush border shedding (2 points), tubular shape (2 points), and exfoliated cells in the lumen of the renal tubules (1 point). Meanwhile, renal damage and inflammation were scored according to the proportion of renal parenchyma by PAS staining, as not obvious (0 points), <10 % (1 point), 10–25 % (2 points), 25–50 % (3 points), or more than 50 % (4 points).

2.5. Inflammasome stimulation

BMDMs were plated at 1×10^6/mL in 6-well plates in DMEM supplemented with FBS and penicillin–streptomycin solution. The cells were primed with 500 ng/mL LPS for 3 h the next day, followed by a 0.5 h treatment with compound 15a and subsequently with ATP (2.5 mM) or nigericin (10 μM) for 0.5 h or Alum (300 μg/mL) for 4 h.

2.6. Western blot and co-immunoprecipitation

The experimental protocol was executed as previously described [22]. In brief, 400 μL of cell culture supernatants, 400 μL of methanol, and 100 μL of chloroform were mixed with vibration and centrifuged at

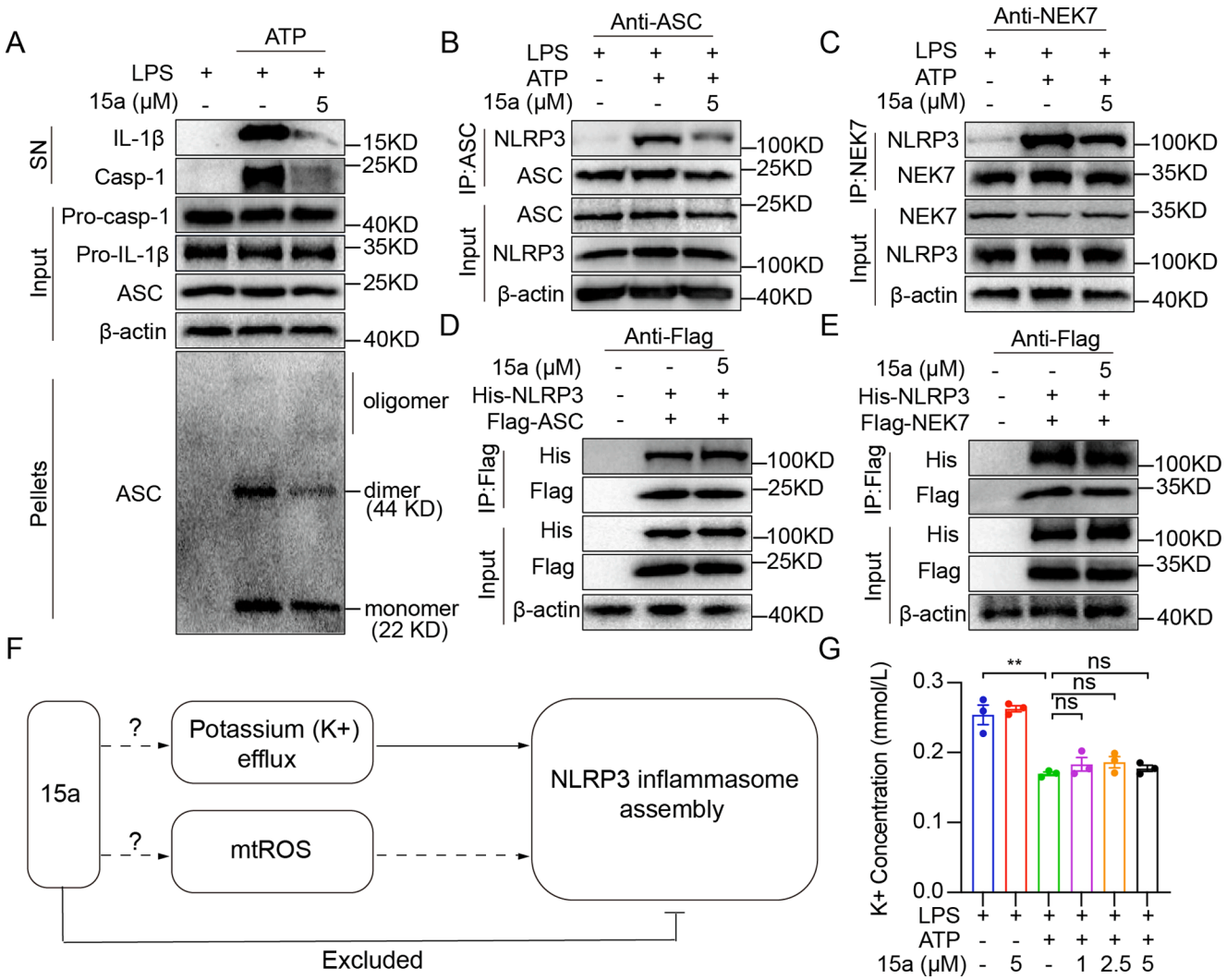

Fig. 2. Compound 15a targets upstream effectors of NLRP3-inflammasome assembly in BMDMs. (A) Western blot of ASC oligomerization of LPS-primed BMDMs in 0.5 % Triton X-100 treated with or without 15a (5 μM) for 0.5 h and stimulated with ATP for 0.5 h. **(B)** Western blot for evaluating NLRP3–ASC interaction in LPS-primed BMDMs treated with or without 15a for 0.5 h and stimulated with ATP for 0.5 h. **(C)** Co-IP with NEK7 antibody and western blotting analysis to evaluate the NLRP3–NEK7 interaction in LPS-primed BMDMs treated with or without 15a (5 μM) for 0.5 h and stimulated with ATP for 0.5 h. **(D)** Co-IP with Flag antibody and western blot for evaluating NLRP3–ASC interaction in HEK-293 T cells transfected with high expression plasmid and treated with 15a (5 μM). **(E)** Co-IP with Flag antibody and western blot for evaluating NLRP3–NEK7 interaction in HEK-293 T cells transfected with high expression plasmid and treated with 15a (5 μM). **(F)** Schematic diagram of the upstream regulators of NLRP3 inflammasome formation. **(G)** Detection of potassium (K +) efflux in LPS-primed BMDMs treated with 15a (1, 2.5, and 5 μM) for 0.5 h and stimulated with ATP for 0.5 h. Data are presented as the mean ± SEM, n = 3; **P < 0.01, ***P < 0.001; ns, not significant.

12000 × g for 10 min at 4 °C. After discarding the upper phase, 400 μL of methanol was added into the tube. After vortexing and another centrifugation (12000 × g for 10 min at 4 °C), the protein precipitate was dissolved in 50 μL of 2 × loading buffer.

Total proteins from cells and tissues were lysed separately in lysis buffer (cat# AR0103, Boster, Wuhan, China) and Tissue Protein Extraction Reagent (cat# AR0101, Boster, Wuhan, China) and centrifuged at 12000 × g for 0.5 h at 4 °C. The amount of cytosol proteins (25-45μg) was measured using bicinchoninic acid (BCA; cat# 23225, Thermo Scientific). The samples were resolved and separated by 12 % SDS-PAGE, and then transferred to polyvinylidene-fluoride membranes for immunoblot analysis.

For co-immunoprecipitation assays, cytosolic proteins were extracted using lysis buffer after inflammasome stimulation. The extracts (300 μg) were incubated with decoy antibodies overnight at 4 °C, and protein A + G agarose beads were added into the samples at 4 °C for 6 h. After being washed 6 times with PBS, the proteins were eluted with SDS loading buffer at 100 °C and subjected to immunoblot analysis.

2.7. ASC oligomerization assay

BMDMs were lysed with a lysis buffer (0.5 % Triton X-100, protease inhibitor cocktail, and PBS). The precipitate was resuspended in PBS after centrifugation, and 2 mmol/mL suberic acid bis (3-sulfo-*N*-hydroxysuccinimide ester) sodium salt (BS3; cat# S855494, Macklin, Shanghai, China) was added to crosslink the oligomers at 37 °C for 0.5 h. Then the pellets were resuspended in SDS sample loading buffer and analyzed by immunoblotting after centrifugation.

2.8. Detection of intracellular potassium

BMDMs were plated in 6-wells plates and prepared using a regular protocol. The plate was washed with 0.9 % normal saline and the cells were lysed with ultrapure water at 37 °C. Samples were collected after centrifugation and tested for potassium concentration by using an AU5800 Clinical Chemistry Analyzer (Beckman Coulter, Indianapolis, IN, USA).

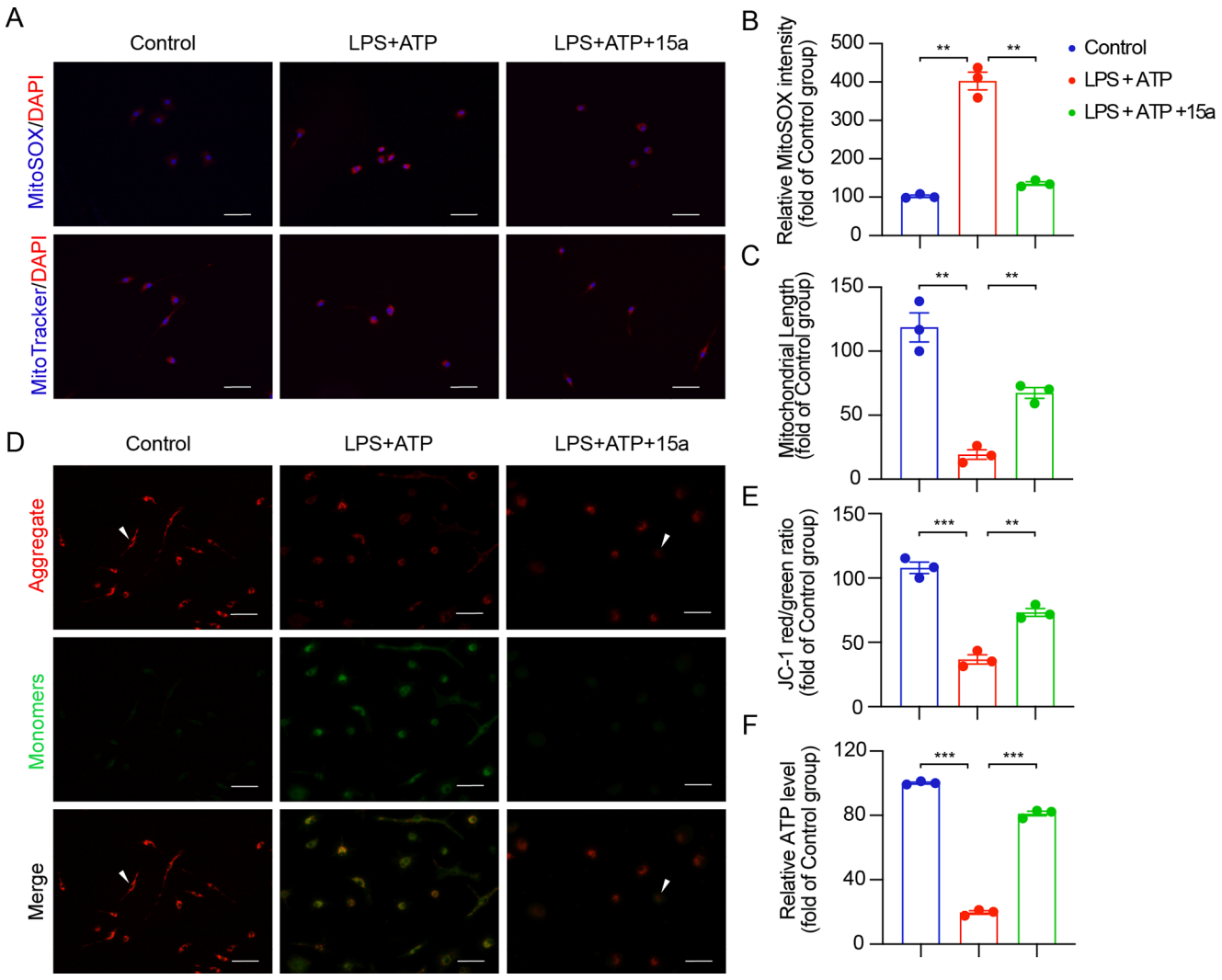

Fig. 3. Compound 15a reduces mtROS production and attenuates mitochondrial damage in BMDMs. (A-C) Fluorescence staining of LPS/ATP-challenged BMDMs treated with compound 15a using MitoSOX or MitoTracker, as well as DAPI **(A)**. Scale bar = 50 μm. Fluorescence intensity **(B)** and the length of the mitochondria **(C)** were quantified using Image J and Prism 9. **(D, E)** The mitochondrial membrane potential was measured using JC-1 **(D)** and quantified by the ratio of red and green fluorescence intensity using Image J and Prism 9 **(E)**. Scale bar = 50 μm. **(F)** Detection of ATP in LPS-primed BMDMs treated with compound 15a (5 μM) for 0.5 h and stimulated with ATP for 0.5 h. Data are presented as the mean ± SEM, n = 3; $^{**}P < 0.01$, $^{***}P < 0.001$; ns, not significant.

2.9. Lactate dehydrogenase (LDH) assay

The assay of LDH in BMDMs with compound 15a was performed using the LDH Cytotoxicity Assay Kit (cat# C0016, Beyotime, Shanghai, China) by following the manufacturer's instructions.

2.10. Elisa

The pyroptosis indicator interleukin-1β (IL-1β) was detected using an enzyme-linked immunosorbent assay (ELISA) kit (cat# 88–7013-77, Invitrogen) by following the manufacturer's instructions.

2.11. MitoSOX, MitoTracker, and JC-1 staining

MitoSOX, MitoTracker, and JC-1 staining assays were performed using assay kits (MitoSOX, cat# M36008, Invitrogen, Carlsbad, CA, USA; MitoTracker; cat# C1049B, Beyotime, Shanghai, China; Mitochondrial membrane potential assay kit with JC-1, cat# C0026, Beyotime, Shanghai, China). Experiments were performed according to the manufacturer's instructions. Briefly, after inflammasome stimulation, BMDMs were incubated with assay reagents at the recommended concentrations for 0.5 h. The BMDMs were subsequently washed with PBS and fixed in paraformaldehyde for 10 min. Finally, the cells were counterstained with DAPI and imaged using an epifluorescence microscope (Nikon, Tokyo, Japan).

2.12. Immunofluorescence staining

Immunofluorescence staining of kidney tissues was performed on 5-μm frozen sections. Briefly, sections were fixed in rectisol for 1 h, blocked with 1 % BSA for 1 h, and incubated with primary antibodies at 4 °C overnight. After being washed thrice with PBS on 2nd day, the sections were incubated with fluorophore-conjugated secondary antibodies for 1 h at 37 °C. The sections were counterstained with DAPI and imaged using an epifluorescence microscope (Nikon, Tokyo, Japan).

2.13. Isolation of mitochondria

Tissue mitochondrial extraction kits were used for mitochondrial isolation from the kidney according to the manufacturer's instructions. Briefly, the mitochondria and cytosol were isolated by differential centrifugation and stored in a storage solution containing

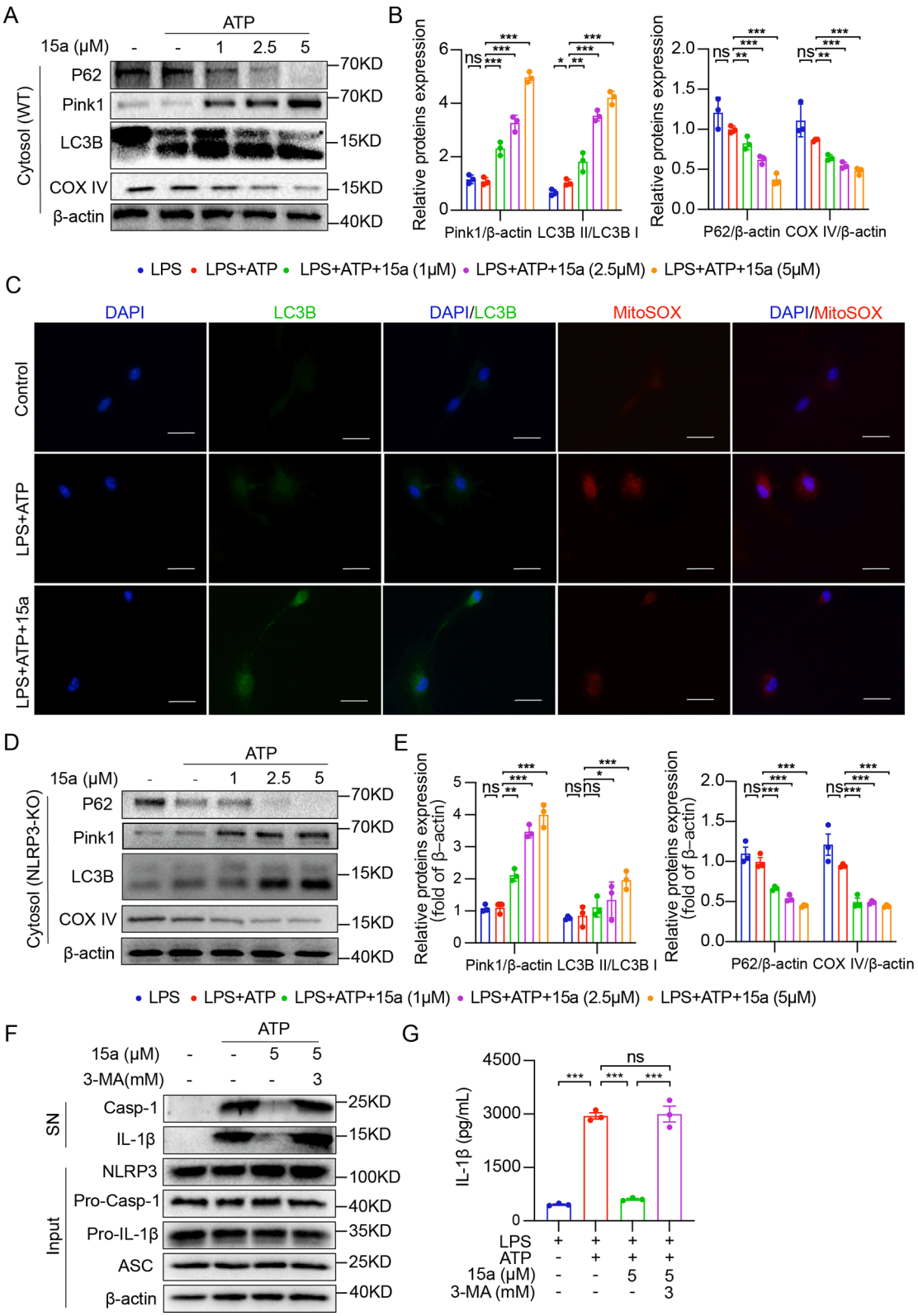

Fig. 4. Compound 15a activates mitophagy to reduce mtROS in BMDMs. (A, B) LPS-primed WT BMDMs were treated with various doses of compound 15a (1, 2.5, and 5 μM) for 0.5 h and subsequently stimulated with ATP for 0.5 h. Western blot analysis of Pink1, *P*62, COX IV, LC3B, and β-actin in lysates of BMDMs **(A)**. Quantified data are normalized to β-actin and LC3B is quantified with LC3B II/LC3B I **(B)**. **(C)** Representative images of fluorescence staining of LC3B, MitoSOX and DAPI in BMDMs. Scale bar = 25 μm. **(D, E)** LPS-primed NLRP3-KO BMDMs were treated with compound 15a (5 μM) for 0.5 h and subsequently stimulated with ATP for 0.5 h. Western blotting analysis of Pink1, *P*62, COX IV, LC3B, and β-actin in lysates of BMDMs **(D)**. Quantified data are normalized to β-actin and LC3B is quantified with LC3B II/LC3B I **(E)**. **(F, G)** LPS-primed BMDMs were treated with or without 3-MA (3 mM) for 3 h and subsequently treated with compound 15a (5 μM) for 0.5 h, followed by ATP stimulation for 0.5 h. Western blot assay of cleaved IL-1β and casp-1 in the supernatant **(F)** and ELISA detection of cleaved IL-1β in the supernatant **(G)**. Data are presented as the mean ± SEM, n = 3; $^{**}P < 0.01$, $^{***}P < 0.001$; ns, not significant.

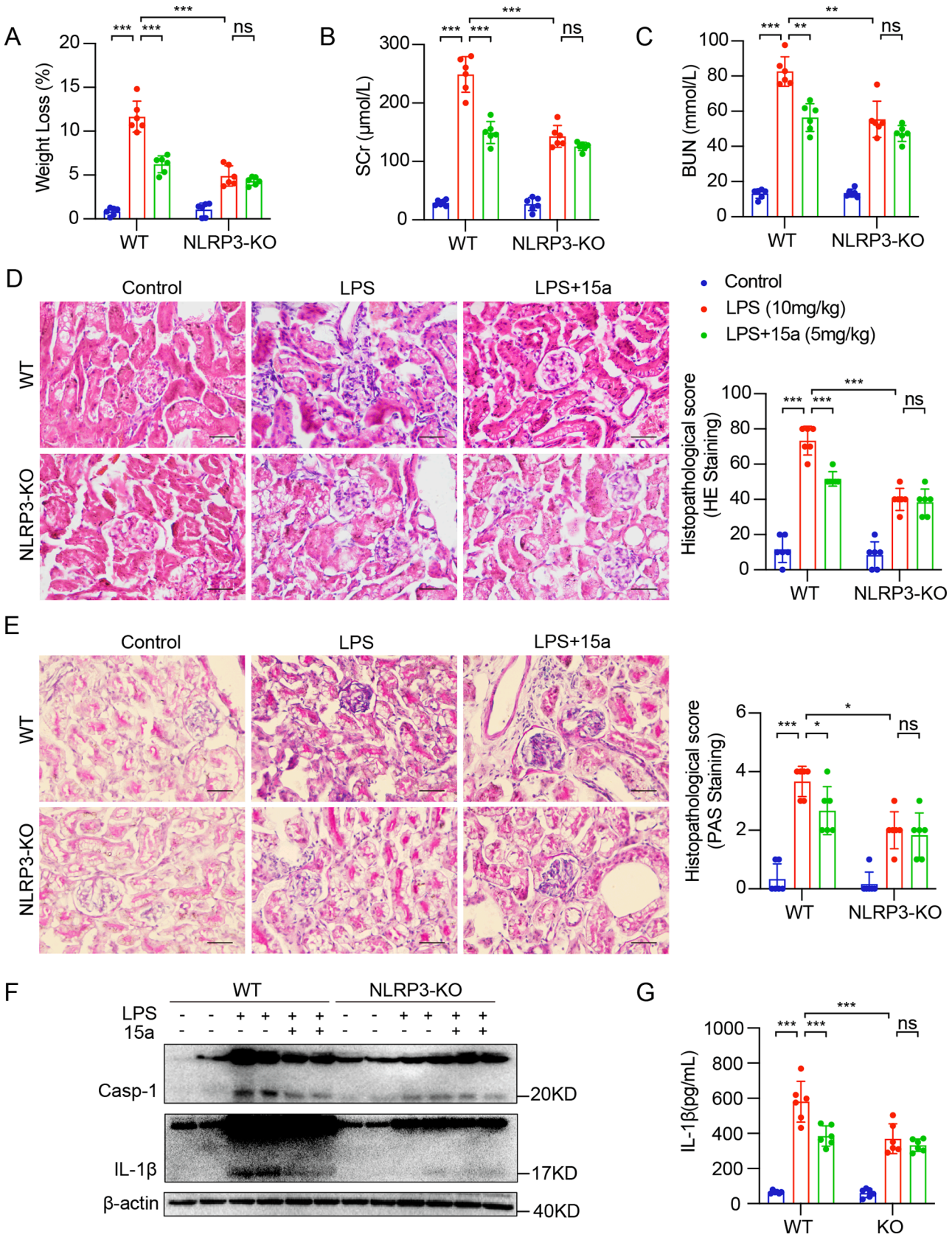

Fig. 5. Compound 15a alleviates LPS-induced ATN by inhibiting NLRP3-mediated inflammation. (A) Percentage of weight loss in WT and NLRP3-KO mice (n = 6 mice per group). **(B, C)** Detection of BUN **(B)** and Cre **(C)** in the serum of both WT and NLRP3-KO mice with ATN. **(D, E)** Representative images of mouse kidneys stained with H&E **(D)** and PAS **(E)**. Scale bar = 50 μm. Renal inflammation and pathological alterations were scored. **(F)** Western blotting for Casp-1, IL-1β, and β-actin in tissue homogenates from the kidneys of WT and NLRP3-KO mice. **(G)** Serum level of IL-1β in ATN mice was assessed using ELISA. Data are presented as the mean ± SEM, n = 6 per group; *p < 0.05, **p < 0.01, ***p < 0.001, ns, not significant.

phenylmethylsulfonyl fluoride for immunoblot analysis.

2.14. Statistical analysis

All experiments are randomized and blinded. All results are presented as the mean ± standard error of the mean (SEM). Statistical significance of differences between groups were determined using Student't-test or one-way ANOVA multiple comparisons in GraphPad Prism 8 (GraphPad, San Diego, CA, USA). One-way ANOVA followed by Dunnett's post hoc test was used to compare more than two groups of data. Differences were considered statistically significant at $P < 0.05$.

3. Results

3.1. Compound 15a significantly inhibits NLRP3-mediated pyroptosis in BMDMs.

Compound 15a was designed based on Tan IIA, which has been shown to inhibit the NLRP3 inflammasome [24–26]. First, by comparing the level of IL-1β released in the supernatant medium, we found that compound 15a showed a much stronger anti-inflammatory effect than the lead compound Tan IIA at the same concentration (5 μM) (Fig. 1B). To further validate the inhibitory effect of compound 15a on NLRP3 inflammasome activation, LPS-primed BMDMs were treated with compound 15a (1, 2.5, and 5 μM), followed by an ATP challenge, which was a second signal and was essential for NLRP3 inflammasome assembly. Compound 15a dose-dependently inhibited the release of cleaved-caspase-1 and cleaved-IL-1β (Fig. 1C-D). Meanwhile, compound 15a decreased LDH release in LPS/ATP-challenged BMDMs (Fig. 1E). Furthermore, we found that compound 15a (5 μM) exhibited a similar inhibitory effect on cleaved-caspase-1 and cleaved-IL-1β stimulated by other NLRP3 agonists, including nigericin and alum (Fig. 1F-G). These results demonstrated that compound 15a inhibited NLRP3 inflammasome activation and NLRP3-mediated pyroptosis in BMDMs.

3.2. Compound 15a targets upstream effectors of NLRP3-inflammasome assembly in BMDMs.

To elucidate the underlying mechanisms of the inhibitory effect of compound 15a against NLRP3 inflammasome, we validated that compound 15a at 5 μmol/mL decreased the oligomerization of ASC induced by ATP in BMDMs (Fig. 2A). We further found that compound 15a significantly inhibited the interaction between ASC and NLRP3, as well as interaction between NEK7 and NLRP3, in LPS/ATP-challenged BMDMs (Fig. 2B-C). However, pretreatment with compound 15a failed to block the interactions between the proteins in HEK-293 T cells transfected with ASC/NLRP3 or NEK7/NLRP3, respectively (Fig. 2D-E). These results indicated that compound 15a inhibited the activation of NLRP3 inflammasome by exerting the effects on the upstream regulators of NLRP3 inflammasome formation, rather than directly targeting NLRP3 inflammasome itself. Several factors, mainly including potassium (K^+) and mtROS (Fig. 2F), were reported to be upstream regulators of NLRP3 inflammasome assembly [19,24]. The ATP-gated cation channel P2X7R, which is engaged in extracellular ATP and membrane pore formation caused by bacterial toxins, promotes K + efflux. By measuring the K^+ concentration of the outflow, we excluded the inhibitory effect of compound 15a on the K^+ efflux (Fig. 2G), indicating that mtROS might be involved in effect of compound 15a.

3.3. Compound 15a reduces mtROS production and attenuates mitochondrial damage in BMDMs.

The generation of ROS, 90 % of which is generated from mitochondria, is widely considered another indispensable factor in inflammasome activation [19]. To determine the regulatory effect of compound 15a on mtROS and mitochondria, LPS/ATP-challenged BMDMs were incubated in MitoSOX or MitoTracker after pretreatment with compound 15a (5 μM) to separately label mitochondrial superoxide or mitochondrial morphology, respectively. The exposure of BMDMs to LPS/ATP for total 4 h caused a significant enhancement of MitoSOX-positive spots and a significant reduction in mitochondrial length in BMDMs, while these changes were reversed in cells treated with compound 15a (Fig. 3A-C). Additionally, the Mitochondrial Permeability Transition Pore (MPTP) was examined by JC-1 staining and the ATP detection was determined using an ATP assay kit (Fig. 3D-F). The number of dysfunctional mitochondria was increased in LPS/ATP-challenged BMDMs, but significantly decreased in the compound 15a-treated group. These results demonstrated that compound 15a significantly reduced the level of mtROS and mitochondrial injuries induced by LPS/ATP in BMDMs.

3.4. Compound 15a activates mitophagy to reduce mtROS in BMDMs.

The mechanisms and effectors of regulating mtROS are very complex, and mitochondrial autophagy is also one of the important ways [27]. We investigated whether mitophagy is involved in the anti-pyroptosis and mitochondria-protective effects of compound 15a. We first examined the levels of mitophagy-associated proteins in BMDMs. Compared with the vehicle-treated group, LPS/ATP-challenged BMDMs pretreated with compound 15a exhibited remarkably high expression of microtubule-associated protein light chain 3B II (LC3B II) and a markedly decreased level of SQSTM1 (*P*62), an essential adaptor that identifies and delivers specific proteins and organelles to autophagosomes for degradation. In addition, Cytochrome *c* oxidase IV (COX IV), localized in the inner membrane of mitochondria and recognized as a molecular marker of mitochondria, was decreased and the PTEN-induced kinase 1 (Pink1) was increased in the compound 15a-treated BMDMs (Fig. 4A-B). Additionally, co-fluorescence staining of LC3B and MitoSOX showed that compound 15a significantly increased the expression of LC3B and reduced the robust generation of mtROS in LPS/ATP-challenged BMDMs (Fig. 4C). Interestingly, similar results were observed in NLRP3-KO BMDMs (Fig. 4D-E). In contrary, the anti-NLRP3 and anti-pyroptosis effects of compound 15a was eliminated in LPS/ATP-challenged BMDMs in the presence of 3-MA (3 mM), an inhibitor of autophagy (Fig. 4F-G), indicating that the anti-NLRP3 effect of compound 15a was mediated by mitophagy. These results suggested that compound 15a promoted mitophagy to protect mitochondria and reduce mtROS accumulation, leading to the inhibition of NLRP3 inflammasome activation in LPS/ATP-treated BMDMs.

3.5. Compound 15a alleviates LPS-induced ATN by inhibiting NLRP3-mediated inflammation

To verify whether compound 15a attenuated ATN through inhibiting NLRP3, we established well-accepted ATN models in both wide-type (WT) and NLRP3-KO mice as previously reported [9]. WT and NLRP3-KO mice were administered compound 15a (5 mg/kg, i.p.) and then injected with LPS (10 mg/kg, i.p.) to induce ATN, respectively. As depicted in Fig. 5A, WT mice injected with only LPS lost more body weight than those injected with compound 15a. Both compound 15a administration and NLRP3 gene knockout significantly lowered the levels of SCr and BUN in mice with LPS challenge (Fig. 5B-C). In addition, H&E and PAS staining of the kidney tissue showed that compound 15a treatment ameliorated renal inflammation and edema in the kidneys of LPS-induced WT mice (Fig. 5D-E). Moreover, western blot assay showed that LPS-induced group showed markedly increased levels of cleaved caspase-1 and mature IL-1β in kidney tissues, while these changes were reversed by compound 15a treatment (Fig. 5F). ELISA data also suggested that compound 15a remarkable reversed LPS-induced increase of serum IL-1β in mice (Fig. 5G). As expected, we observed the protective effects of NLRP3 deficiency against LPS-induced ATN phenotypes in mice (Fig. 5A-G). These results indicated that compound 15a produces a protective effect against LPS-induced ATN by inhibiting

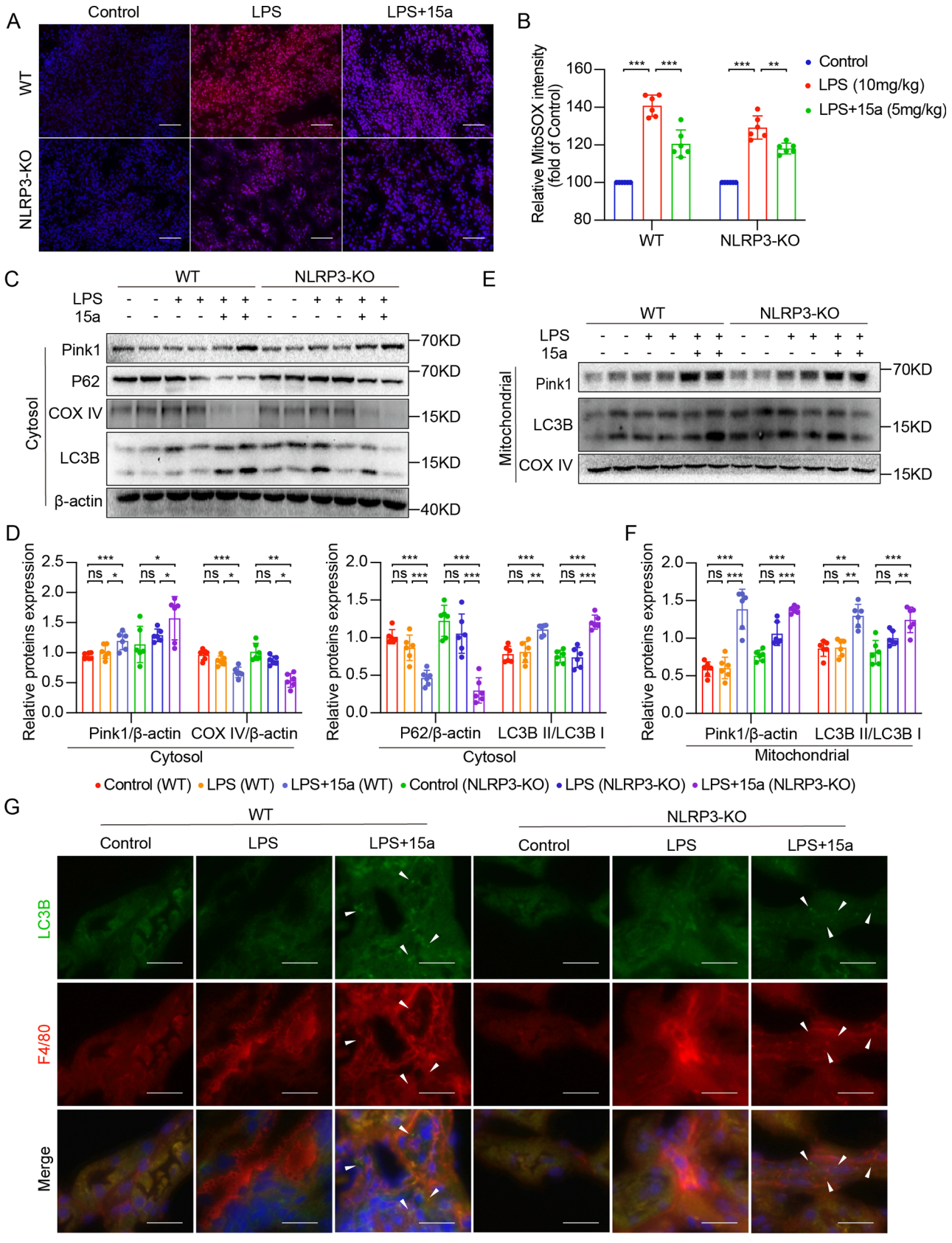

Fig. 6. Compound 15a promotes mitophagy and reduces mtROS in LPS-induced ATN mouse kidney. (A, B) Representative images and quantification of MitoSOX staining **(A)**. Scale bar = 50 μm. Quantification of MitoSOX staining in different groups of ATN mice **(B)**. **(C, D)** Immunoblot analysis of Pink1, *P*62, LC3B, and COX IV in the cytoplasm **(C)**. Quantified data were normalized to β-actin and LC3B was quantified with LC3B II/LC3B I **(D)**. **(E, F)** Immunoblot analysis of Pink1 and LC3B in the mitochondria **(E)**. Pink1 was normalized to β-actin and LC3B was quantified with LC3B II/LC3B I **(F)**. **(G)** Representative images of

immunofluorescence double-labeled LC3B and F4/80. Scale bar = 50 μm. Data are presented as the mean ± SEM, n = 6 per group; *p < 0.05, **p < 0.01, ***p < 0.001, ns, not significant.

the activation of NLRP3 inflammasome in mice.

3.6. Compound 15a promotes mitophagy and reduces mtROS in LPS-induced ATN mouse kidney

To further explore whether compound 15a inhibited NLRP3 inflammasome activation by promoting mitophagy in vivo, we first examined the level of mtROS in kidney tissues using MitoSOX. LPS challenge significantly enhanced renal mtROS generation, while compound 15a remarkably decreased the mtROS production (Fig. 6A-B). Also, the relative levels of proteins involved in mitophagy, including Pink1, *P*62, LC3B, and COX IV, were analyzed in mouse kidney tissues by western blotting. Compared with LPS-challenged group, treatment with compound 15a led to increased Pink1 and LC3B-II/LC3B-I levels and reduced *P*62 level, indicating mitophagy activation (Fig. 6C-D). The level of the mitochondrial protein COX IV, which reflects mitochondrial content, decreased in the compound 15a-treated group (Fig. 6C-D). Furthermore, we isolated mitochondria from the cytoplasm and verified that compound 15a could enhance the activation of mitophagy, as evidenced by increased Pink1 and LC3B-II/LC3B-I levels (Fig. 6E-F). In addition, to prove that compound 15a acted on macrophages to ameliorate LPS-induced ATN, we detected mitophagy in macrophages by co-labeling LC3B and F4/80 (Fig. 6G). Immunofluorescence showed more expression of LC3B around the positive spots of F4/80 in the group treated with compound 15a than in the LPS group and the Control group (Fig. 6G). We also examined the level of mtROS and the activation of mitophagy in NLRP3-KO mice with LPS-induced ATN. NLRP3 gene knockout did not affect LPS-induced renal mtROS and mitophagy profile in mice (Fig. 6A-G), conforming a downstream position of NLRP3. As expected, compound 15a still promotes mitophagy and reduces mtROS in LPS-induced NLPR3-KO mouse kidney (Fig. 6A-G).

3.7. Compound 15a inhibits NLRP3-mediated inflammation by promoting mitophagy in FA-induced ATN mouse model

We also tested the protective effect of compound 15a in another ATN mouse model induced by FA injection. In consistent with the results in LPS-induced ATN model, FA-induced ATN phenotypes was also greatly reversed by treatment with compound 15a (Fig. 7A-E). In addition, compound 15a treatment considerably reduced IL-1β and caspase-1 expression in the kidneys (Fig. 7F) and IL-1β secretion in the serum (Fig. 7G), indicating that compound 15a inhibited NLRP3 inflammasome activation in vivo. NLRP3 deficiency also suppressed FA-induced ATN in mice by itself (Fig. 7A-G). Further, compound 15a treatment reduced the production of mtROS (Fig. 8A-B), increased the level of mitophagy-related proteins LC3B II and Pink1, and decreased the expression of *P*62 and COX IV (Fig. 8C-F) in FA-challenged mouse kidney tissues. Concordantly, a higher level of LC3B-II expression was observed in the macrophages of compound 15a-treated mouse kidney tissues (Fig. 8G). NLRP3 gene knockout did not affect the profile of renal mtROS and mitophagy in FA-induced mice, no matter with compound 15a administration (Fig. 8A-G). These data further validated the anti-NLRP3 effect of compound 15a on ATN via promoting mitophagy and blocking mtROS in FA-induced mice.

4. Discussion

In this study, a Tan IIA analogue, compound 15a, showed a stronger anti-pyroptosis effect than Tan IIA in BMDMs. We determined its anti-pyroptosis mechanism in BMDMs and its protective effects in ATN mouse models. We showed that the mitophagy pathway was a vital regulatory point through which 15a promoted clearance of damaged mitochondria to reduce mtROS production and subsequently inhibit NLRP3 inflammasome assembly and pyroptosis in BMDMs. Moreover, compound 15a significantly alleviated ATN and reduced renal inflammation and injury in mouse models induced by LPS or FA challenge through the indicated mechanisms. Collectively, we focused on the effect of compound 15a on the interaction between mitophagy and NLRP3 inflammasome assembly, which alleviated inflammation in BMDMs; thus, we clarified the renoprotective effect of compound 15a by preventing renal tubular epithelial cell damage caused by excessive inflammatory toxicity. This study provided compound 15a as a new candidate for the treatment of ATN and indicated that the mitophagy-mtROS-NLRP3-pyroptosis axle in macrophages might present a potential target to discover new therapies for ATN. Our main findings are summarized in the Graphic Abstract.

Previous studies have revealed that Tan IIA suppressed NLRP3 inflammasome by inhibiting endoplasmic reticulum stress [26] and inactivating succinate dehydrogenase [28]. However, the mechanism underlying the anti-inflammasome effect of Tan IIA is not yet fully understood. To our knowledge, this is the first study to demonstrate that the structural derivative of Tan IIA has stronger inhibitory effects on the NLRP3 inflammasome than Tan IIA. Additionally, we found that compound 15a suppressed NLRP3-mediated inflammation by promoting mitophagy and eliminating mtROS overload in pathological conditions. Further, we confirmed that 15a inhibited NLRP3 inflammasome activity and ATN phenotypes in both LPS and FA-induced ATN mouse models by promoting mitophagy. However, it is still unclear how compound 15a activates mitophagy, which needs to be elucidated in the future study.

So far, most reports on ATN have focused on the tubular epithelial cells. However, recent studies have shown that activation and recruitment of inflammatory cells is one of the most important pathological features of ATN. The number of macrophages in the kidney increases sharply under pathological conditions of ATN [5]. According to previous reports, PAMPs increase in the interstitial microenvironment of kidney tissue during early tubular injury. Resident macrophages in the kidneys are activated by PAMPs through innate pattern-recognition receptors including NLRP3, resulting in the secretion of pro-inflammatory cytokines and chemokines and subsequent inflammatory injuries, such as pyroptosis [29]. Our results showed that compound 15a attenuated ATN by reducing pro-inflammatory cytokine release and pyroptosis via inhibiting NLRP3 inflammasome activation in macrophages. We acknowledge that the prophylactic approach in our experiments may be a limitation of this study. A treatment approach in our future studies may strengthen the pharmacological effect of 15a.

In this study, we showed compound 15a could not affect the NEK7-NLRP3-ASC interaction in 293 T cells, indicating that it did not directly target NLRP3 inflammasome complex. Further, we excluded the effect of compound 15a on potassium profile, following which we focused on the interaction between compound 15a and mtROS. mtROS are generated from the electron transport chain in the damaged mitochondria. Research has shown that mtROS initiated NLRP3 inflammasome assembly. The NLRP3 activation induced by ATP, Candida albicans, and various crystals (MSU, asbestos, and silica) could be reversed by the removal of mtROS [15,30]. According to our results, ATP-induced mtROS levels in BMDMs decreased remarkably with compound 15a treatment. We observed that the low production of mtROS resulted in the inactivation of NLRP3 inflammasome assembly and the reduction of the downstream cleaved caspase-1 and IL-1β. Studies have revealed that the excessive accumulation of mtROS resulted in oxidative stress and mitochondrial dysfunction. With the up-regulation of mtROS and subsequent oxidative stress, transcription factors in the nucleus were activated, and transcription of mitophagy-corresponding proteins including LC3B and *P*62 was initiated,

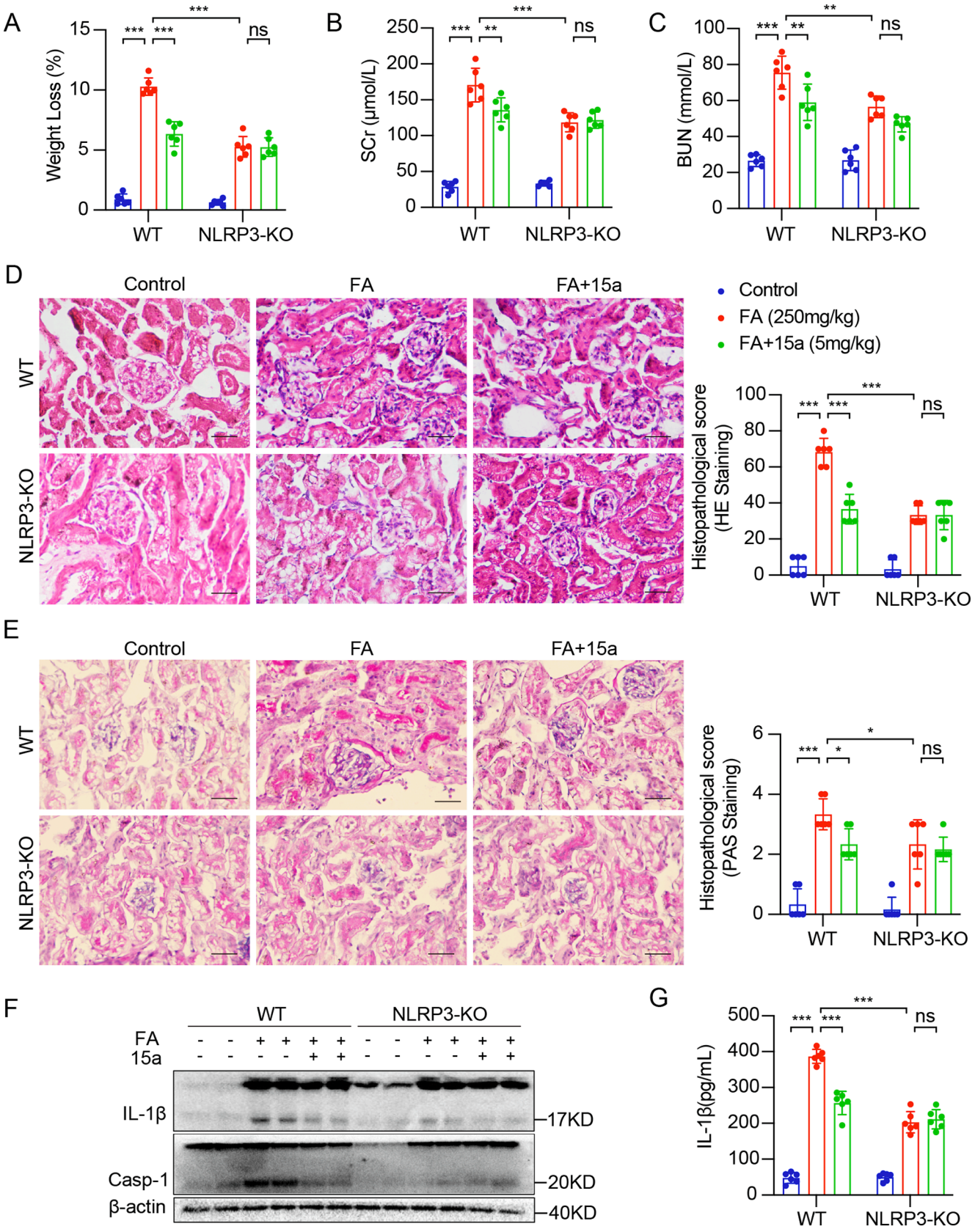

Fig. 7. Compound 15a inhibits NLRP3-mediated inflammation by promoting mitophagy in FA-induced ATN mouse model. (A) Percentage of weight loss both in WT and NLRP3-KO mice (n = 6 mice per group). **(B, C)** Detection of BUN **(B)** and Cre **(C)** in the serum of both WT and NLRP3-KO mice with ATN. **(D, E)** Representative images of mouse kidneys stained with H&E **(D)** and PAS **(E)**. Scale bar = 50 μm. Renal inflammation and pathological alteration were scored. **(F)** Western blotting of casp-1, IL-1β, and β-actin of tissue homogenates from the kidney of WT and NLRP3-KO mice. **(G)** Serum level of IL-1β in the ATN mice was assessed using ELISA. Data are presented as the mean ± SEM, n = 6 per group; *p < 0.05, **p < 0.01, ***p < 0.001, ns, not significant.

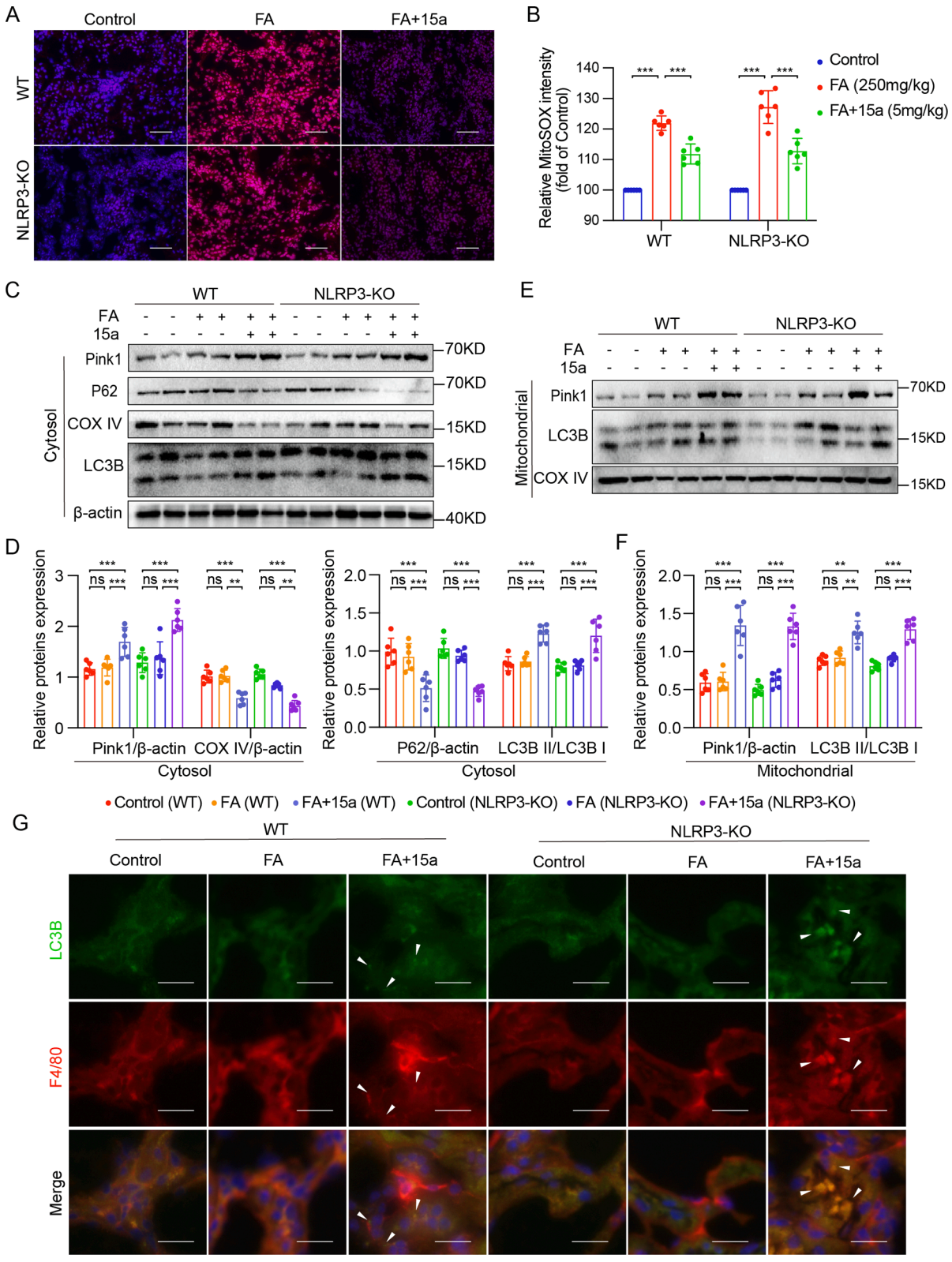

Fig. 8. Compound 15a inhibits NLRP3-mediated inflammation by promoting mitophagy in FA-induced ATN mouse model. (A, B) Representative images and quantification of MitoSOX staining **(A)**. Scale bar = 50 μm. Quantification of MitoSOX staining in different groups of ATN mice **(B)**. **(C, D)** Immunoblot analysis of Pink1, *P*62, LC3B, and COX IV in the cytoplasm **(C)**. Quantified data were normalized to β-actin and LC3B was quantified with LC3B II/LC3B I **(D)**. **(E, F)** Immunoblot analysis of Pink1 and LC3B in the mitochondria **(E)**. Pink1 was normalized to β-actin and LC3B was quantified with LC3B II/LC3B I **(F)**. **(G)** Representative images of immunofluorescence double-labeled LC3B and F4/80. Scale bar = 50 μm. Data are presented as the mean ± SEM, n = 6 per group; *p < 0.05, **p < 0.01, ***p < 0.001, ns, not significant.

resulting in the engagement of mitophagy. Our data showed that compound 15a promoted mitophagy, resulting in the down-regulation of the mtROS-NLRP3 inflammasome pathway both in vitro and in vivo.

To further validate the mitophagy-promoting effect of the compound, we used 3-MA, an class III PI3K inhibitor of autophagy, to block the initiation of autophagy in BMDMs. There are three classes of PI3Ks participating in the regulation of autophagy. The class III PI3K contributes to the initiation and progression of autophagy. With the treatment of 3-MA, the initiation of autophagosome was abrogated. Our results showed that the effect of compound 15a on NLRP3 inflammasome was reversed by 3-MA intervention. Based on our study, it will be interesting to further evaluate the mitophagy-promoting effects of 15a in the future study.

5. Conclusion

In summary, this study demonstrated that the Tan IIA-derived compound 15a exhibited a therapeutic effect in ATN by inhibiting pyroptosis in either LPS- or FA-induced mice. In terms of mechanism, compound 15a activated mitophagy to improve mitochondrial quality and reduce mtROS, resulting in anti-NLRP3 inflammasome assembly in BMDMs. NLRP3 knockout reversed the renoprotective effects of compound 15a in LPS- or FA-induced ATN mice, but did not affect the mitophagy activation and mtROS reduction in compound 15a-treated mice. Collectively, these studies clearly showed an important role of macrophage mitophagy-mtROS-NRLP3-pyroptosis axle in the pathogenesis of ATN and suggested that compound 15a could potentially target this signaling pathway to treat ATN.

Data Viability.

The datasets generated during the current study are available from the corresponding author on reasonable request.

CRediT authorship contribution statement

Jiahao Chen: Investigation, Methodology, Formal analysis, Data curation, Visualization, Writing – original draft. **Wu Luo:** Methodology, Investigation, Formal analysis, Data curation, Visualization. **Chenghong Hu:** Methodology, Investigation, Formal analysis, Data curation. **Miao Ren:** Methodology, Investigation, Formal analysis, Data curation, Visualization. **Haowen Xu:** Investigation, Methodology. **Xiangwei Xu:** Resources, Data curation. **Weifeng Li:** Resources, Data curation. **Yue Chen:** Resources, Data curation. **Jingjing Shao:** Resources, Data curation. **Zhongxiang Xiao:** Investigation, Methodology. **Xinting Lv:** Conceptualization, Supervision, Project administration. **Guang Liang:** Conceptualization, Supervision, Project administration, Funding acquisition, Writing – original draft.

Declaration of Competing Interest

The authors declare that they have no known competing financial interests or personal relationships that could have appeared to influence the work reported in this paper.

Data availability

No data was used for the research described in the article.

Acknowledgments

This study was supported by the National Natural Science Foundation of China (81930108 to G.L. and 82000793 to W.L.), the Natural Science Foundation of Zhejiang Province (LBY21H070001 to Z.X., and LY22H070004 to W.L.), and Wenzhou Science Project in China (Y20210213 to W.L.).

Appendix A. Supplementary material

Supplementary data to this article can be found online at https://doi.org/10.1016/j.intimp.2023.110065.

References

[1] M.L. Esson, R.W. Schrier, Diagnosis and treatment of acute tubular necrosis, Ann. Intern. Med. 137 (9) (2002) 744–752.
[2] H.I. Han, L.B. Skvarca, E.B. Espiritu, A.J. Davidson, N.A. Hukriede, The role of macrophages during acute kidney injury: destruction and repair, Pediatr. Nephrol. 34 (4) (2019) 561–569.
[3] S.C. Huen, L.G. Cantley, Macrophage-mediated injury and repair after ischemic kidney injury, Pediatr. Nephrol. 30 (2) (2015) 199–209.
[4] M.Z. Zhang, B. Yao, S. Yang, L. Jiang, S. Wang, X. Fan, H. Yin, K. Wong, T. Miyazawa, J. Chen, I. Chang, A. Singh, R.C. Harris, CSF-1 signaling mediates recovery from acute kidney injury, J. Clin. Invest. 122 (12) (2012) 4519–4532.
[5] Q. Cao, D.C. Harris, Y. Wang, Macrophages in kidney injury, inflammation, and fibrosis, Physiol. (Bethesda) 30 (3) (2015) 183–194.
[6] L. Xu, The Role of Myeloid Cells in Acute Kidney Injury and Kidney Repair, Kidney360 2 (11) (2021) 1852–1864.
[7] N. Li, J. Chen, P. Wang, H. Fan, S. Hou, Y. Gong, Major signaling pathways and key mediators of macrophages in acute kidney injury (Review), Mol. Med. Rep. 23 (6) (2021).
[8] M. Benoit, B. Desnues, J.L. Mege, Macrophage polarization in bacterial infections, J. Immunol. 181 (6) (2008) 3733–3739.
[9] S.N. Heyman, W. Lieberthal, P. Rogiers, J.V. Bonventre, Animal models of acute tubular necrosis, Curr. Opin Crit. Care 8 (6) (2002) 526–534.
[10] Z. Liu, X. Wang, Y. Wang, M. Zhao, NLRP3 inflammasome activation regulated by NF-kappaB and DAPK contributed to paraquat-induced acute kidney injury, Immunol. Res. 65 (3) (2017) 687–698.
[11] J. Ni, L. Jiang, G. Shen, Z. Xia, L. Zhang, J. Xu, Q. Feng, H. Qu, F. Xu, X. Li, Hydrogen sulfide reduces pyroptosis and alleviates ischemia-reperfusion-induced acute kidney injury by inhibiting NLRP3 inflammasome, Life Sci. 284 (2021), 119466.
[12] S.J. Song, S.M. Kim, S.H. Lee, J.Y. Moon, H.S. Hwang, J.S. Kim, S.H. Park, K. H. Jeong, Y.G. Kim, Rhabdomyolysis-Induced AKI Was Ameliorated in NLRP3 KO mice via alleviation of mitochondrial lipid peroxidation in renal tubular cells, Int. J. Mol. Sci. 21 (22) (2020).
[13] F.S. Sutterwala, S. Haasken, S.L. Cassel, Mechanism of NLRP3 inflammasome activation, Ann N Y Acad. Sci. 1319 (1) (2014) 82–95.
[14] B.Z. Shao, Z.Q. Xu, B.Z. Han, D.F. Su, C. Liu, NLRP3 inflammasome and its inhibitors: a review, Front Pharmacol. 6 (2015) 262.
[15] N. Kelley, D. Jeltema, Y. Duan, Y. He, The NLRP3 Inflammasome: an overview of mechanisms of activation and regulation, Int. J. Mol. Sci. 20 (13) (2019).
[16] J. Dan Dunn, L.A. Alvarez, X. Zhang, T. Soldati, Reactive oxygen species and mitochondria: A nexus of cellular homeostasis, Redox Biol. 6 (2015) 472–485.
[17] R. Zhou, A.S. Yazdi, P. Menu, J. Tschopp, A role for mitochondria in NLRP3 inflammasome activation, Nature 469 (7329) (2011) 221–225.
[18] G. Ashrafi, T.L. Schwarz, The pathways of mitophagy for quality control and clearance of mitochondria, Cell Death Differ. 20 (1) (2013) 31–42.
[19] M. Biasizzo, N. Kopitar-Jerala, Interplay Between NLRP3 Inflammasome and Autophagy, Front Immunol. 11 (2020), 591803.
[20] R. Guo, L. Li, J. Su, S. Li, S.E. Duncan, Z. Liu, G. Fan, Pharmacological Activity and Mechanism of Tanshinone IIA in Related Diseases, Drug Des. Devel. Ther. 14 (2020) 4735–4748.
[21] C. Ding, H. Chen, B. Liang, M. Jiao, G. Liang, A. Zhang, Biomimetic synthesis of the natural product salviadione and its hybrids: discovery of tissue-specific anti-inflammatory agents for acute lung injury, Chem. Sci. 10 (17) (2019) 4667–4672.
[22] H. He, H. Jiang, Y. Chen, J. Ye, A. Wang, C. Wang, Q. Liu, G. Liang, X. Deng, W. Jiang, R. Zhou, Oridonin is a covalent NLRP3 inhibitor with strong anti-inflammasome activity, Nat. Commun. 9 (1) (2018) 2550.
[23] M.S. Paller, J.R. Hoidal, T.F. Ferris, Oxygen free radicals in ischemic acute renal failure in the rat, J. Clin. Invest. 74 (4) (1984) 1156–1164.
[24] D. Li, Z. Yang, S. Gao, H. Zhang, G. Fan, Tanshinone IIA ameliorates myocardial ischemia/reperfusion injury in rats by regulation of NLRP3 inflammasome activation and Th17 cells differentiation, Acta Cir. Bras. 37 (7) (2022) e370701.
[25] H.L. Li, T. Li, Z.Q. Chen, L. Li, Tanshinone IIA reduces pyroptosis in rats with coronary microembolization by inhibiting the TLR4/MyD88/NF-kappaB/NLRP3 pathway, Korean J. Physiol. Pharmacol. 26 (5) (2022) 335–345.
[26] Y. Li, Y. Fu, J. Sun, J. Shen, F. Liu, B. Ning, Z. Lu, L. Wei, X. Jiang, Tanshinone IIA alleviates NLRP3 inflammasome-mediated pyroptosis in Mycobacterium tuberculosis-(H37Ra-) infected macrophages by inhibiting endoplasmic reticulum stress, J. Ethnopharmacol. 282 (2022), 114595.
[27] J.H. Schofield, Z.T. Schafer, Mitochondrial reactive oxygen species and mitophagy: a complex and nuanced relationship, Antioxid. Redox. Signal 34 (7) (2021) 517–530.
[28] Q.Y. Liu, Y. Zhuang, X.R. Song, Q. Niu, Q.S. Sun, X.N. Li, N. Li, B.L. Liu, F. Huang, Z.X. Qiu, Tanshinone IIA prevents LPS-induced inflammatory responses in mice via

inactivation of succinate dehydrogenase in macrophages, Acta. Pharmacol. Sin. 42 (6) (2021) 987–997.
[29] H.J. Anders, M. Ryu, Renal microenvironments and macrophage phenotypes determine progression or resolution of renal inflammation and fibrosis, KidneyInt. 80 (9) (2011) 915–925.
[30] K.E. Lawlor, J.E. Vince, Ambiguities in NLRP3 inflammasome regulation: is there a role for mitochondria? Biochim. Biophys. Acta. 1840 (4) (2014) 1433–1440.